Fluorescence Study of Arene Probe Microenvironment in the Intraparticle Void Volume of Zeolites Interfaced with Bathing Polar Solvents

Eric H. Ellison,* Deshi Moodley, and Joseph Hime

Department of Chemistry and Biochemistry, University of Mississippi, University, Mississippi 38677

Received: November 29, 2005; In Final Form: January 13, 2006

Fluorescence methodologies have been utilized to examine micropolarity, intramolecular motion, and singlet quenching in the intraparticle void volume of zeolites X, Y, and ultrastable Y (USY) interfaced with bathing polar solvents. Micropolarity was assessed from the 3-to-1 band ratio (III/I) of the fluorescence spectrum of pyrene (PY) and from λ_{max} of the fluorescence spectrum of 1-pyrenecarboxaldehyde (1-PCA). In zeolites bathed in anhydrous solvents, both PY and 1-PCA reported increased micropolarity according to the trend USY < bulk solvent < NaX ≈ NaY. For example, in NaY (USY), III/I ranged from 0.44 (0.98) in acetonitrile to 0.52 (1.34) in *n*-hexanol, compared to 0.60, 1.06, and 1.62 in bulk acetonitrile (ACN), *n*-hexanol, and *n*-hexane, respectively. The polarity studies reveal that the ionic nature of NaX and NaY and the hydrophobic nature of USY strongly influence the microenvironment of the arene despite the presence of desorbing polar solvents. Constraints on intramolecular motion were examined in polar-solvated NaX through measurements of the fluorescence lifetime of *trans*-stilbene. Lifetimes ranged from 113 ps in NaX-ACN to 671 ps in NaX-*tert*-butyl alcohol. The latter value is close to that observed in bulk glycerol. Diffusion-controlled quenching of PY fluorescence by O_2 and a series of nitrocompounds dissolved in solvents bathing the zeolite was examined by a time-resolved approach. For all of the quenchers and solvents studied, quenching was more efficient in USY compared to NaX and NaY. Interestingly, the rate of O_2 quenching in USY-MeOH was only 12 times lower than that in bulk MeOH. In contrast, in NaY-MeOH and NaX-MeOH the rate of O_2 quenching was too low to be measured. The rate constants in these systems were therefore taken as the rate constant for diffusion-controlled quenching of trapped electrons measured previously. These values were 600 times and 10^5 times lower than the rate of fluorescence quenching in USY-MeOH, respectively. The O_2 quenching studies show that dispersive interactions of polar solvents with the cavity walls dominate in USY because of the hydrophobic nature of the USY surface. In NaX and NaY, stronger ion−dipole and hydrogen bonding interactions dominate and lead to more restricted access and lowered quenching efficiency. Perrin (or static) quenching of pyrene fluorescence was also examined to infer the concentration of nitromethane (NM) in the void volume of NaX and NaY bathed in MeOH, ACN, or H_2O. The results indicate that access of NM to the interior of NaY is more inhibited in ACN compared to MeOH, presumably because of the higher dipole moment of ACN and its resulting stronger association with the zeolite surface. At similar levels of static quenching equated to a similar NM concentration in the zeolite, dynamic quenching by NM varied by no more than a factor of 2 in all systems compared. This implies that the rate of NM diffusion in solvated zeolite interiors is similar regardless of zeolite or solvent properties. In contrast to O_2 diffusion in zeolites, NM exhibits a high dipole moment and can therefore migrate through polar-solvated zeolite apertures by adsorbing to the zeolite. Overall, the results of this study show a close relationship between the behavior of probes and quenchers in the confines of polar-solvated zeolite interiors and the chemical properties of the zeolite. Differences between weakly and strongly interacting surfaces are revealed clearly in the results.

Introduction

Photochemists have explored heterogeneous reaction media as a means to more effectively control the behavior of excited states and photogenerated intermediates. One means of control has been to place reactant molecules in the intraparticle void volume of zeolites. Zeolites are crystalline aluminosilicates having a microporous (d_p < 2 nm) void volume and high surface-to-volume ratio. Probably the most fascinating feature of zeolites is their intraparticle void structure. The void spaces of zeolites are of molecular size and only slightly larger than the molecules that can be included in them. The inclusion of photochemical reactants in zeolite void spaces has been shown to promote selectivity, energy transfer, and electron transfer through constraints on molecular motion resulting from confinement in small pores and through electronic polarization resulting from molecular association with zeolite exchangeable cations. Several review articles are available on the subject of photochemistry in zeolites.[1−15] Of modern interest is the use of zeolites to spatially organize molecules and create organic−inorganic hybrid materials or devices with supramolecular functionality.

Methodologies that probe the behavior of molecules in zeolites at the molecular level provide the detailed information needed to understand and develop new uses for zeolites. Fluorescence methodologies have long been used to examine

* Corresponding author. Tel: (662) 915-7875. Fax: (662) 915-7300. E-mail: eellison@olemiss.edu.

10.1021/jp056926g CCC: $33.50
Published on Web 02/11/2006

the microenvironment of probe molecules in heterogeneous media, zeolites included. There is great interest in knowing the local environment of molecules at interfaces. Fluorescence-based approaches have been used to describe micropolarity,[16−20] intramolecular motion,[21,22] dimer and complex formation,[17,18,23−29] and singlet quenching[17,18,30−33] in zeolite cavities. Of the fluorescent molecular probes used to study zeolites, pyrene has been particularly useful. The use of pyrene is ubiquitous in studies of heterogeneous systems such as polymer films, silica surfaces, and surfactant assemblies, to name a few.[34−36] A report in 1977 by Kalyanasundarum and Thomas on the Ham effect in pyrene fluorescence was the first to demonstrate the utility of using pyrene for the characterization of heterogeneous systems, in particular, lipid and surfactant assemblies.[37] The Ham effect is a general effect based in selection rules governing electronic transitions in aromatic molecules.[38] For pyrene fluorescence, the Ham effect is reflected in the 3-to-1 ratio (or III/I), or the ratio of intensities of the third vibronic band to the first vibronic band (or 0−0 transition). Intensity enhancements in the 0−0 band occur as a result of specific solute−solvent dipole−dipole coupling, whereas the third vibronic band intensity is unaffected by such interactions. As III/I increases, micropolarity decreases. In bulk solvents, greater correlation is observed between III/I and dipole moment (μ), as compared to III/I and dielectric constant (ϵ). Another useful aspect of pyrene is its long fluorescence lifetime. In solution, the fluorescence lifetime of most arene probes is a few nanoseconds or shorter, whereas that of pyrene is several hundred nanoseconds. The long lifetime provides greater flexibility in quenching studies, especially in more rigid systems where diffusion is inhibited. Convenience of the fluorescence approach is also an advantage. Many types of heterogeneous systems studied are not optically clear and therefore do not lend themselves very well to quenching studies by flash photolysis or transient absorption spectroscopy.

Our studies of adsorbate photophysics on porous solids have revealed an interesting feature concerning the association of pyrene and other arenes with zeolites interfaced with bathing polar solvents. We refer to such zeolites as polar-solvated zeolites, or PSZ. In these studies, self-supported disks of zeolites NaX and NaY, when loaded with pyrene, were found to remain brightly fluorescent upon UV-excitation for at least months after submerging the disks in polar solvents such as methanol or acetonitrile. This effect is unusual compared to what is typically observed for mesoporous solids such as silica gel. For example, pyrene-loaded disks of 60-Å silica gel become nonfluorescent within minutes of exposure to the same solvents. The fact that pyrene can be loaded rather easily into the cavities of NaX and NaY by adsorption from solution but cannot be extracted with desorbing polar solvents at room temperature is intriguing. We have reported the nature of extraction of pyrene and other arene probes from PSZ recently.[39] The current study seeks to describe the nature of PSZ as a reaction medium by a photophysical approach. Quenching of arene excited states and microenvironmental polarity or rigidity in the void volume of zeolites interfaced with bathing polar solvents are of primary interest. Previous studies of arene photophysics in zeolites have also explored the role of polar solvation. A common approach has been to add less-than-cage-filling amounts of water to the zeolite from the vapor phase. The current study differs from the majority of these previous studies through focus on bathing amounts of polar solvents and not just water. A wide variety of polar organic solvents have been tested.

In the zeolites X and Y devoid of solvent, the interaction of aromatic species with exchangeable cations leads to the so-called π-cation effect in which exchangeable cations behave as Lewis acids.[23,27] For pyrene the result is distortion in the π-electronic distribution, intensity enhancements of the 0−0 fluorescence band, and low values of III/I. In fact, some of the lowest III/I ever recorded have been observed under evacuated conditions in dehydrated zeolites.[32] In contrast, in PSZ, aromatic interactions with zeolite cations are greatly modified as a result of shielding by polar solvents. Such effects can be advantageous because the interaction of aromatics with zeolite cations is not always favorable. Because pyrene occupies a significant fraction of the supercage volume, then most of the solvent pyrene encounters in PSZ is a type of interfacial solvent associated directly with the zeolite or zeolite cations. Such a medium is unique and worth exploration.

In the current study, microenvironmental polarity in PSZ was assessed by using pyrene and 1-pyrenecarboxaldehyde (or 1-PCA) as fluorescent probes. 1-PCA is structurally similar to pyrene, but operates as a polarity probe by a different mechanism explained below. Microenvironmental rigidity in PSZ was assessed through measurements of the fluorescence lifetime of *trans*-stilbene, which comments on the rate of trans-to-cis isomerization. Pyrene fluorescence was also used to examine diffusion-controlled singlet quenching by O_2 and a series of nitrocompounds varying in size and dissolved in solvents bathing the zeolite. For all of these measurements and when possible, a comparison of results in zeolites X, Y, and ultrastable Y (or USY) was made. Zeolites X and Y are synthetic forms of the naturally occurring mineral Faujasite, the structure and properties of which are described in detail by Breck.[40] Compared to zeolite Y, zeolite X has a higher aluminum content, is more negatively charged, and contains more exchangeable cations. USY is a type of nonionic zeolite. Although the pore structure of USY is practically identical to that of zeolites X and Y, its ionic content is much lower as a result of chemical treatments designed to remove aluminum. Many interesting properties of USY have been reported, including low affinity for polar adsorbates such as water and alcohols and high affinity for nonpolar adsorbates such as hydrocarbons.[41] Some refer to USY as hydrophobic. However, USY can be dispersed or suspended in water quite easily, much like zeolites X or Y. In actuality, the hydrophobicity description originates from differences in affinity of adsorbates for USY from the vapor phase. For example, the water content of USY is <1% after standing for several days in normal laboratory air. In contrast, NaX and NaY are much more hygroscopic and imbibe 25% of their weight in water under the same conditions.

Experimental Section

Powdered forms of zeolites NaX and NaY with chemical compositions $Na_{80}Al_{80}Si_{112}O_{384}$ (Si/Al = 1.4) and $Na_{55}Al_{55}Si_{137}O_{384}$ (Si/Al = 2.5), respectively, were obtained from Aldrich or UOP. Both zeolites were stirred in excess 1 M $NaNO_3$(aq) and rinsed thoroughly with ultrapure Millipore water. Lithium and potassium ion exchange was carried out by repeated exposure to 1 M nitrate salt solutions at 70 °C followed by rinsing. USY (CBV-901) was obtained from Zeolyst International and used as received. Fluorescent probes were purified either by recrystallization in ethanol or by column chromatography using silica gel as the stationary phase and cyclohexane as the eluent. Nitrocompounds were obtained from Aldrich and used as received. Anhydrous solvents were purchased and stored over activated Type 3A molecular sieves prior to use. Abbreviations for solvents used in the text are given as follows: methanol (MeOH), ethanol (EtOH), *n*-butanol (*n*-BuOH), *tert*-butyl

alcohol (*t*-BuOH), acetonitrile (ACN), tetrahydrofuran (THF), dimethylformamide (DMF), dimethyl sulfoxide (DMSO), dichloromethane (DCM), and cyclohexane (C_6H_{12}).

Self-supported zeolite disks were utilized as the test medium and were prepared by compression of 10−25 mg of powder at 3000 lbs pressure in a die cell. The pressure used was the lowest possible that yielded a working disk. Pyrene (PY), 1-pyrenecarboxaldehyde (1-PCA), and *trans*-stilbene (*t*St) were loaded into zeolites X and Y as follows according to a previous procedure.[39] The disks were dehydrated in air at 550 °C for at least 5 min, cooled under a flowing stream of dry N_2, transferred to solutions of probe in cyclohexane, and agitated for several hours. For loadings <0.05 s^{-1}, 90% or greater adsorption was observed. The loaded disks were transferred to an evacuable cell and evacuated for 30 min with mild heating (125 °C) or until the vacuum pressure reached 2−3 mTorr. A previous study has shown this treatment to be effective at removing water from the zeolite.[32] Pyrene-loaded disks were quickly transferred in air (<5 s exposure) to 2.5 mL of polar solvent and agitated for at least 30 min in sealed 20 mL glass vials. Rates of extraction in polar solvents were measured as described previously by placing samples in a Teflon-capped quartz cuvette (1-cm path length) and measuring the increase in absorbance in solution at variable time intervals.[39]

Loading of probes onto USY required a special coating procedure because of weak adsorption. For USY, probes were loaded by allowing a solution of the probe in pentane to evaporate in air from disks, followed by evacuation for 30 min with mild heating (125 °C). Samples were then exposed to polar solvents as described above. Extraction of pyrene and 1-PCA from polar-solvated USY was not significant over short time intervals (<24 h) and was similar to that observed previously for pyrene in NaY.[39] Heating the zeolite following the coating procedure places significant amounts of pyrene in the intraparticle void volume where pyrene is retained following submersion of samples in polar solvents.

Fluorescence was measured by steady-state and time-resolved approaches, employing 45° front-face excitation and collection. A PTI QM-4 steady-state spectrofluorometer was used to collect fluorescence spectra. Decay profiles of pyrene fluorescence were collected following excitation with 0.5-ns pulses from a PTI GL-3300 nitrogen laser (λ = 337.1 nm). The emission was passed through a monochromator and detected with a photosensor having a rise time of 0.78 ns. A Tektronix TDS-3052B digitizing oscilloscope (500 MHz bandwidth) was used to capture and store the decay profiles. Decay profiles of *t*St fluorescence were collected following excitation with 40-ps pulses from a Continuum PY-61 passively mode-locked Nd:YAG laser operating at 266 nm. A Hamamatsu phototube (R1328U-53) having a rise time of 60 ps was used as the detector. Signals were captured by using a 5-GHz transient digitizer (Tektronix SCD5000). The rise time of the setup was measured to be 85 ps. All fluorescence lifetimes were assessed from fits to decay profiles by using a NLLS fitting algorithm.

Results and Discussion

Microenvironmental Polarity. The fluorescence spectrum of pyrene included in the void volume of NaX, NaY, or USY submerged in EtOH is shown in Figure 1. Each spectrum was normalized so that III/I is given by the intensity of band III. The spectral broadening observed in NaX-EtOH was atypical of the results. All other systems showed band shapes or resolution similar to that in solution, including NaX in EtOH

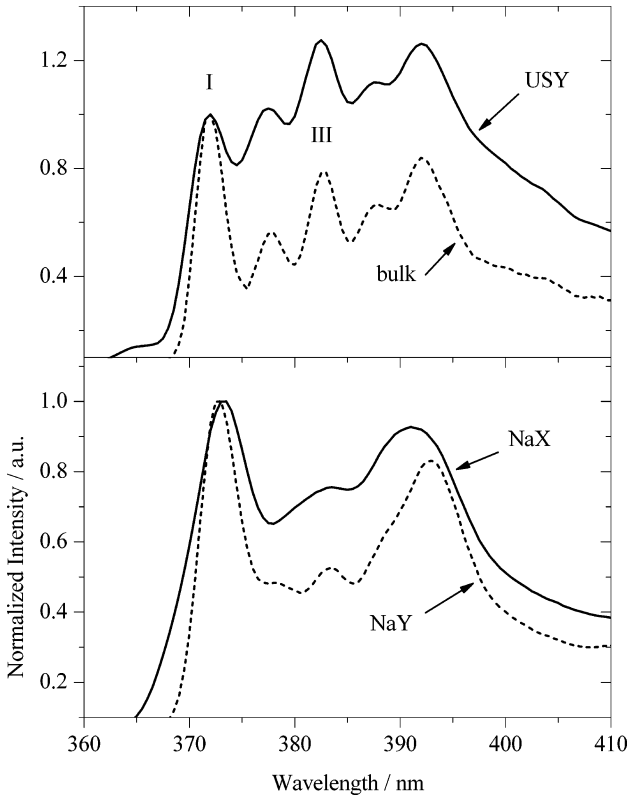

Figure 1. Pyrene fluorescence spectrum in bulk EtOH and in zeolites bathed in EtOH. λ_{ex} = 337 nm.

TABLE 1: Pyrene III/I and Fluorescence Lifetimes in Polar-Solvated Zeolites[a]

solvent	bulk	NaX	NaY	USY
none	n/a	0.46	0.36	0.96
		118	76	71
MeOH	0.76	0.69	0.49	1.19
	263	172	176	335
EtOH	0.77	0.75	0.55	1.27
	352	192	207	273
n-BuOH	1.02	0.59	0.51	1.26
	339	149	156	354
t-BuOH	1.02	0.54	0.61	1.30
	417	173	168	339
1-hexanol	1.06	0.52	0.52	1.34
	413	153	166	397
ethylene glycol	0.63	0.59	0.71	1.12
	295	186	219	303
acetonitrile	0.60	0.47	0.44	0.98
	292	146	170	380
DMSO	0.53	0.47	0.52	1.10
	247	111	129	308
DMF	0.56	0.51	0.53	1.02
	295	131	160	230
water	0.59	0.51	0.67	0.88
	184	181	167	318

[a] Upper value is III/I, lower value is lifetime (ns). Pyrene loading = 0.002 sc^{-1}.

containing small amounts of water. Table 1 lists values of III/I and τ_f in anhydrous solvents. All systems were N_2-bubbled prior to measurement. The decay profiles in NaX and NaY were single exponential with minor deviations in a few cases. Those in USY were double exponential and are described in more detail below. Decay profiles in evacuated systems (solvent = none) were heterogeneous. Therefore, these decay profiles were analyzed according to the Gaussian model, which conveniently yields the average decay time. Details of the Gaussian approach are described elsewhere.[42−44]

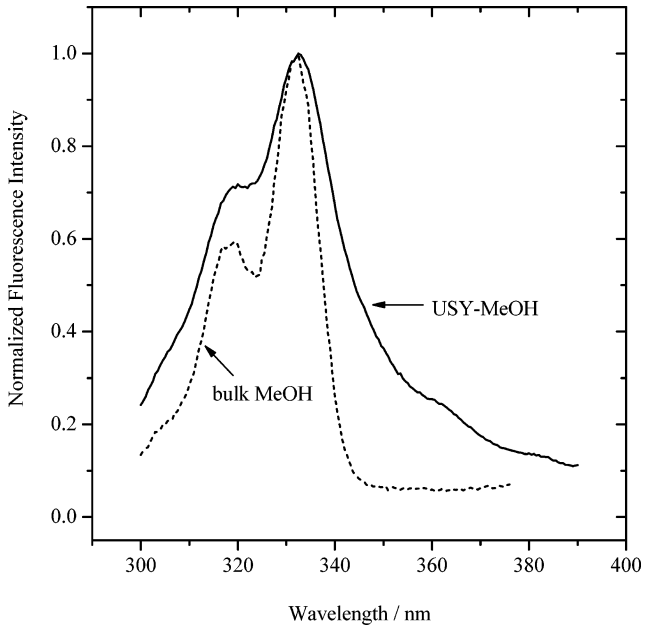

Figure 2. Excitation spectrum for pyrene fluorescence in USY-MeOH and in bulk MeOH. $\lambda_{em} = 395$ nm.

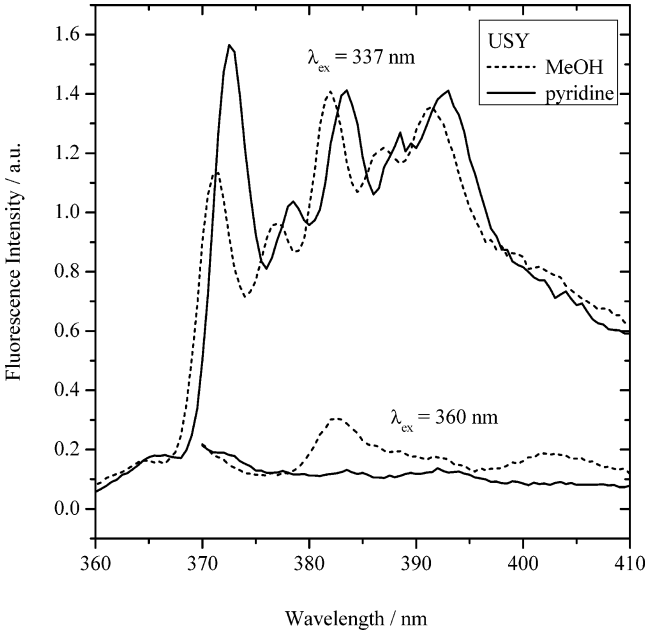

Figure 3. Variation due to λ_{ex} of the pyrene fluorescence spectrum in USY-MeOH and USY-pyridine.

In USY, charge-transfer (CT) fluorescence was observed that was not observed in NaX or NaY. Figure 2 compares fluorescence excitation spectra in USY-MeOH and bulk MeOH. Significant tailing into the visible region can be seen in USY-MeOH. The fluorescence spectrum was also measured by excitation in the tailing band, at $\lambda_{ex} = 360$ nm, and is shown in Figure 3. In this case the fluorescence spectrum is different from the normal pyrene fluorescence spectrum measured by excitation at 337 nm. Previous studies have shown similar fluorescence bands on colloidal TiO_2,[45] silica,[46] and alumina.[47] Therefore, the CT states observed in USY are not unusual. The CT fluorescence was also observed in USY-pentane and USY-cyclohexane.

Figure 3 also shows that the CT band is absent in USY-pyridine. The CT fluorescence could also be eliminated by the addition of 5% pyridine to pentane. These results imply that

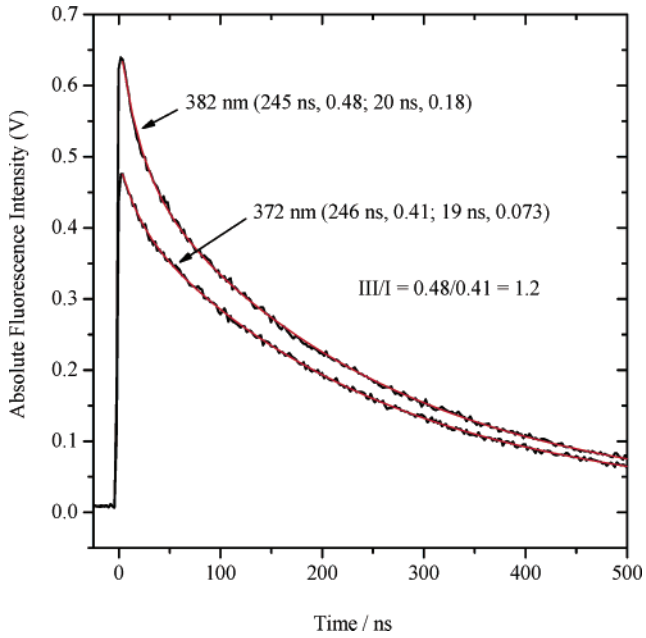

Figure 4. Decay profiles of pyrene fluorescence in air-saturated USY-EtOH following pulsed excitation at 337 nm. Fits to a double exponential model are shown for both decay profiles.

the CT sites are acidic and shielded by pyridine. Further, because the CT fluorescence was also observed in evacuated USY and in USY-pentane before the pyridine was added, the CT effect is reversible and does not originate from a pyrene derivative that might have formed through reactions in the zeolite during sample preparation. Reversibility is expected for CT states. If the pyridine samples were rinsed thoroughly with MeOH or EtOH, then the CT fluorescence returned. Also, 5% pyridine in MeOH or EtOH had no effect on the CT fluorescence. Evidently, MeOH and EtOH are competitive with pyridine for acid sites. Why this is the case is unclear, but it may have to do with solvent structuring and access of pyridine to acid sites.

The CT fluorescence in USY was also revealed in decay profiles of pyrene fluorescence. Figure 4 illustrates decay profiles in air-saturated USY-EtOH. At 382 nm, two decay components were observed with lifetimes of 20 and 245 ns. At 372 nm, the lifetimes were essentially the same, but the amplitude of the shorter component was smaller compared to that at $\lambda_{em} = 382$ nm. The shorter-lived component can be attributed to CT fluorescence because a significant drop in amplitude from 382 to 372 nm is expected based on the CT fluorescence spectrum in Figure 3. The longer-lived component corresponds to the normal pyrene fluorescence. In Table 1, the lifetimes listed for USY are those of the long-lived component in N_2-bubbled systems.

The CT band identified in Figure 3 could add to the intensity of band III without adding to band I and lead to erroneously high values of III/I. However, this effect is not severe. The quantum yield of CT fluorescence is low and therefore makes a small contribution to the steady-state intensity. Regardless, using the decay profiles in Figure 2, III/I in USY-EtOH can be obtained by dividing the amplitude of the longer-lived component at 382 nm by that at 372 nm. From this analysis, III/I = 1.2 and 0.81 in USY-EtOH and bulk EtOH, respectively. These values are not far-removed from those given in Table 1. Indeed, III/I in USY-EtOH is significantly higher than that in bulk EtOH.

The CT effect evident in USY became less significant in longer-chain alcohols. For example, in *n*-butanol and *n*-hexanol where values of III/I were much higher than that in bulk, the

TABLE 2: Effects of Exchangeable Cation and Solvent Water Content on Pyrene III/I and Fluorescence Lifetimes in PSZ

	Li^+		Na^+		K^+			
solvent	X	Y	X	Y	X	Y	USY	bulk
none	0.55	0.47	0.46	0.36	0.39	0.58	0.96	n/a
	37	85	118	76	58	49	71	
C_6H_{12}	0.59	0.39	0.62	0.44	0.49	0.53	1.00	1.75
	48	70	116	75	49	44	234	400
MeOH	0.51	0.66	0.69	0.49	0.52	0.47	1.19	0.76
	139	170	172	176	112	114	401	263
95/5[a]	0.55	0.85	0.59	0.68	0.45	0.45	1.24	0.73
	152	198	174	198	151	127	376	298
75/25[a]	0.58	0.79	0.54	0.72	0.44	0.42	1.16	0.73
	170	150	135	180	149	130	369	340
H_2O	0.58	0.76	0.51	0.67	0.43	0.40	0.88	0.59
	150	167	181	176	140	129	256	184

[a] MeOH/H_2O (v/v).

CT fluorescence was very minor as normalized decay profiles at 372 and 382 appeared virtually identical. The difference between alcohols may be due to size constraints in small cavities. Hydroxyl groups anchor the alcohol to the surface. Longer chain alcohols anchored to the surface occupy more space in the supercage than smaller alcohols anchored to the surface. Therefore, longer chain alcohols create a more rigid environment in the supercage because more of them are associated directly with the zeolite surface. A more fluid medium is therefore expected in smaller alcohols and this allows greater accessibility to the CT site.

The results for USY indicate that pyrene that is not in a CT site experiences significantly lower polarity compared to the bulk solvent bathing the zeolite. This reveals the hydrophobic nature of USY and points out that the USY surface is not shielded completely by desorbing solvents in the small confining pores. Even in USY bathed in solvents with high dipole moments, including anhydrous ACN, DMSO, and DMF, values of III/I were much higher than those in bulk. In evacuated USY, pyrene reflects a more polar environment because of interactions with polar adsorption sites such as hydroxyl groups and a small number of zeolite cations. In polar solvents, these sites are shielded effectively so that pyrene sees the average nonpolar properties of USY. Of further interest was that in USY bathed in saturated aqueous KNO_3 or Na_2SO_4, III/I was essentially the same as that in USY-H_2O. Therefore, the ionic effects observed in zeolites X and Y cannot be duplicated in USY simply by exposure to saturated salt solutions.

To summarize, the III/I data in Table 1 show for NaX and NaY a highly polar microenvironment and little variation in micropolarity because of solvent properties. This points out that polar solvents do not shield pyrene completely from the effects of zeolite cations and pyrene sees a polar solvent and a very polar surface. However, the lifetimes indicate significant decoupling of pyrene from zeolite cations relative to evacuated conditions. In USY, values of III/I were significantly higher than those in bulk solvents and were also more variable with solvent properties compared to NaX and NaY. This points out the hydrophobic nature of the USY surface. Values of III/I in polar-solvated USY are approximately the average of III/I in bulk alcohol and hydrocarbon solvents. Essentially, pyrene sees the average of two environments as predicted for an interface.

Micropolarity was further explored as a function of solvent water content and zeolite exchangeable cation. Table 2 shows the results in MeOH−water mixtures. Additional data showing the effects of water in other polar solvents is listed in Tables S1−S4 of the Supporting Information. In NaY and LiY a significant response to added water, even one percent water, was observed. In NaY, III/I ranged from 0.44 in acetonitrile to 0.99 in 99/1 hexanol/water. In contrast and with few exceptions, there was little response to added water in NaX and USY. The difference between NaX and NaY can be interpreted in terms of the number of wall cations present and more effective shielding of cations by water. In NaX the ionic strength in the supercage is higher than in NaY because of the presence of site III cations. In essence, cationic effects are difficult to avoid in NaX. In NaY, water more effectively shields the site II cations compared to alcohols because water is smaller and more polar. Therefore, at low water contents association of water with zeolite cations is favored over the alcohol. With greater decoupling of pyrene from zeolite cations, the environment of the alcohol becomes more prominent. Less polar alcohols show greater sensitivity to smaller amounts of water because they are less polar and therefore less competitive with water for cations. The results in KY, where there was little response to added water, point out that cation size is a factor. Larger cations such as K^+, which protrude farther into the supercage, are shielded less effectively by water. For the alkali metal ions, the biggest change in cation size occurs from Na^+ to K^+.

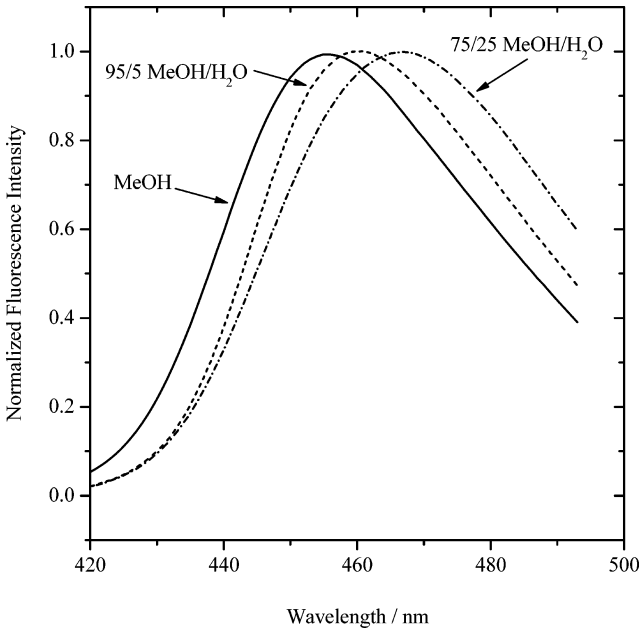

Figure 5. Variability of 1-PCA fluorescence in NaY.

For comparison with the pyrene study, polarity was also examined by using pyrene-1-carboxaldehyde (1-PCA) as a probe. 1-PCA comments on ϵ_s through fluorescence involving (n, π^*) and (π, π^*) states.[48] As ϵ_s increases, the (π, π^*) transition becomes more favorable through solvent interactions with lone pair electrons on the carbonyl group. In polar solvents of $\epsilon_s >$ 10, there is a strong correlation between the fluorescence emission maximum (λ_{max}) and ϵ_s.

Example spectra of 1-PCA fluorescence in polar solvated NaY from which values of λ_{max} were evaluated are illustrated in Figure 5. Bands in PSZ were homogeneous, as in solution. A summary of band maxima in MeOH and EtOH solvents is given in Table 3. Included are values in evacuated NaX and in NaX bathed in cyclohexane. The value in evacuated NaX is identical to that measured in a previous study.[16] Values in evacuated NaY and USY were not included because the spectra were heterogeneous, yielding more than one maximum. The results in alcohols were consistent with the pyrene study. Lower polarity was observed in USY compared to NaX and NaY and the

TABLE 3: Band Maxima (nm) of 1-PCA Fluorescence in Polar-Solvated Zeolites

solvent	NaX	NaY	USY	bulk
none	470			n/a
C_6H_{12}	471			n/a
100/0[a]	457	455	444	451
	459	453	444	445
95/5[b]	460	458	443	452
	460	458	441	449
75/25[b]	465	467	446	454
	467	469	443	450
water	466	472	454	466

[a] Upper value is in MeOH; lower value in EtOH. [b] Alcohol/water mixtures (v/v).

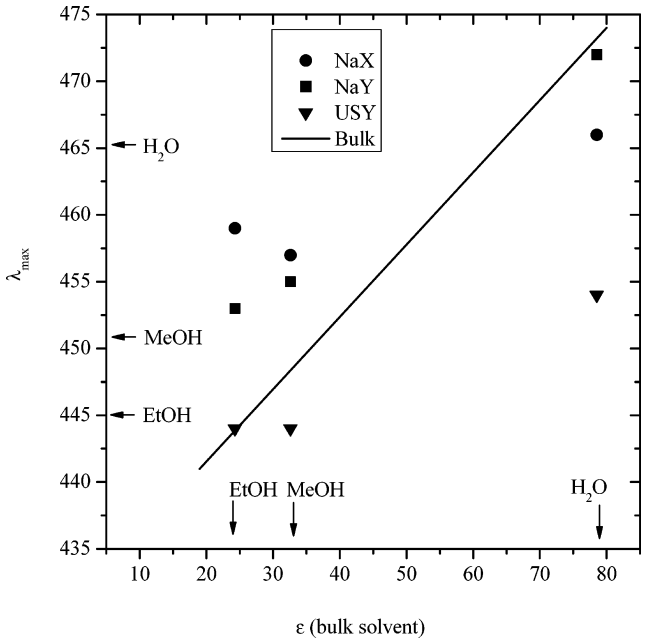

Figure 6. Plots of λ_{max} for 1-PCA fluorescence in PSZ versus ϵ of the bulk solvent bathing the zeolite. The arrows point to either ϵ or λ_{max} in bulk solvents, not in zeolites. The straight line represents the best fit of a plot of λ_{max} in bulk solvents versus ϵ taken from data reported in a previous study.[48]

polarity in bulk solvents was intermediate between that in USY and NaX or NaY. However, in both NaX and NaY the polarity increased with added water unlike the results using pyrene. This indicates that 1-PCA fluorescence is not coupled as strongly the effects of zeolite cations. Perhaps the difference between pyrene and 1-PCA is related to the mode of response. Pyrene III/I correlates more with solvent dipole moment while λ_{max} of 1-PCA correlates more with solvent dielectric constant. Pyrene is more responsive to shielding of zeolite cations by water.

The polarity assessed by using 1-PCA was further clarified according to Figure 6. In Figure 6 values of λ_{max} in zeolites were plotted versus ϵ of the solvent bathing the zeolite. Also given is a best fit of λ_{max} measured previously in a variety of bulk solvents.[48] According to the graph, values for zeolites reflect polarities greater than *n*-propanol for all systems. In NaY-H_2O, λ_{max} was higher than in both bulk water and evacuated NaX. Ramamurthy and co-workers used 1-PCA and other polarity probes to examine polarity in zeolites and described dehydrated NaX and NaY as "superpolar."[16] According to this assessment, NaY in water is also a superpolar medium. Values of III/I for NaX and NaY also show solvent polarity greater than water.

Mobility Constraints. The fluorescence of *trans*-stilbene (*t*ST) can be utilized to gain information about constraints on molecular motion in confining media. Compared to larger rigidity probes, *t*ST can be easily included in the channels and cages of a wide variety of zeolites and is therefore a good probe for zeolites.

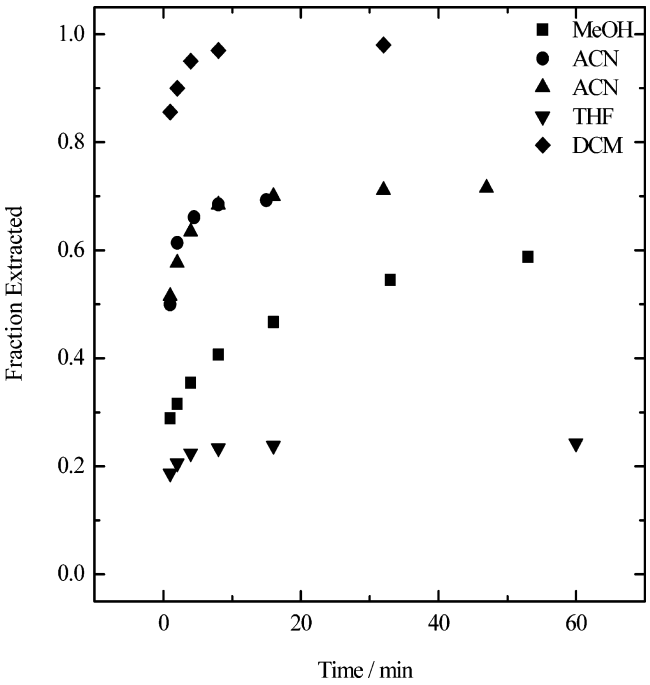

Figure 7. Rates of extraction of *trans*-stilbene from NaX in various solvents.

In bulk solvents, the fluorescence lifetime of *t*ST ($\tau_{f,TS}$) increases with increasing viscosity with $\tau_{f,TS}$ ranging from 66 ps in hexane to 580 ps in glycerin.[21,49−51] The viscosity dependence originates from frictional forces that modulate the twisting motion necessary for isomerization. Two previous studies have probed the fluorescence lifetime of *t*ST within the channels and cages of Faujasite.[21,22] The more recent study has shown essentially no limitations to molecular motion in the cavities of evacuated NaY where $\tau_{f,TS} = 52$ ns. In contrast, in the narrow channels of the zeolite ZSM-5, molecular motion was found to be severly limited at room temperature with $\tau_{f,TS} = 590$ ns. In the present study, the same technique as that used previously[21] was utilized to probe the mobility of *t*ST in PSZ. Unfortunately, rapid and complete extraction of *t*ST from NaY and USY was observed, which prohibited a lifetime analysis of these systems. Therefore, the study was limited to NaX.

The use of *t*ST to probe molecular motion in PSZ requires that it be retained in PSZ. Figure 7 shows the rate of *t*ST extraction from NaX following exposure to polar solvents. As indicated, significant extraction was observed within the first minutes of exposure. In DCM, *t*ST was completely extracted within 30 min. In other solvents, the extraction was not complete and was followed by a much slower rate of extraction. The rapid extraction is difficult to explain, but repeatable as shown for acetonitrile. It could be related to the behavior of solvents in the initial moments of filling the zeolite cavities. Depending on the solvent, there may be more or less space for diffusion in zeolite cavities that places *t*ST on the outer surface. Aside from the rapid extraction, the observed retainment allowed for measurements of $\tau_{f,TS}$ in zeolite cavities. The procedure utilized involved agitating loaded samples for 1 h in polar solvents, followed by a thorough rinse before measurement.

Table 4 lists the average fluorescence lifetimes of *t*ST in NaX, as measured by the Gaussian model. Figure 8 illustrates example decay profiles and Gaussian fits to decay profiles. Noise in the

TABLE 4: Fluorescence Lifetimes of *trans*-Stilbene in NaX[a]

solvent	lifetime/ps
none	see Figure 8
cyclohexane	334
methanol	427
ethanol	464
n-butanol	240
t-butanol	671
glycerol	721
acetonitrile	113
tetrahydrofuran	536

[a] Loading = 0.02 s^{-1}.

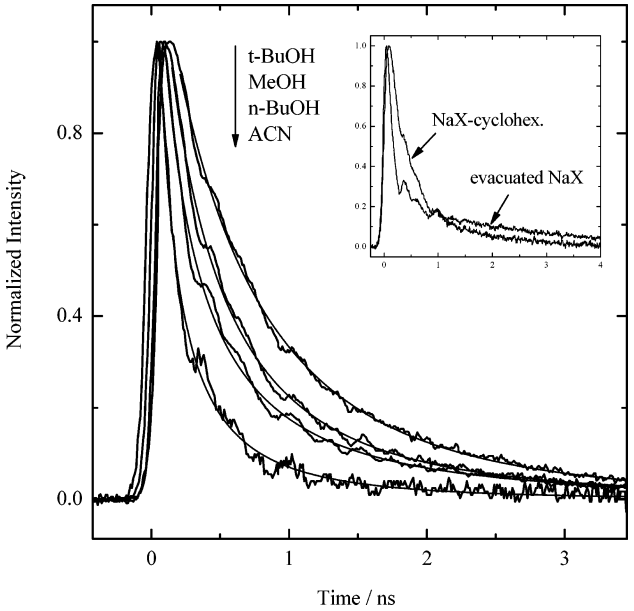

Figure 8. Decay profiles of *trans*-stilbene fluorescence in polar-solvated NaX. The inset shows decay profiles in dehydrated NaX under evacuated conditions and in bathing cyclohexane. Gaussian fits to the decay profiles are shown.

data occurred from reflections or impedance mismatch in the signal cables and connectors but did not severely limit the analysis. The inset of Figure 8 shows the decay profiles in evacuated NaX and NaX bathed in cyclohexane. The decay profile under evacuated conditions exhibited two components: a rapidly decaying, picosecond component consistent with that observed previously in NaY; and a longer-lived nanosecond component that was not observed previously in NaY. The difference between NaX and NaY is probably the result of adsorption to exchangeable cations, with the higher ionicity of NaX causing greater constraints on motion in certain cages. Nevertheless, when cyclohexane was added to the system, the decay profile became more homogeneous and the obvious two-component behavior was no longer observed. In NaX-cyclohexane, *t*ST is adsorbed to the zeolite but the adsorptive interaction is passivated by cyclohexane. The lifetime of 334 ps is only slightly higher than the value of 275 ns observed previously in NaY-cyclohexane.

In polar solvents, *trans*-stilbene is not adsorbed to the zeolite. In the bulky solvent *t*-BuOH, $\tau_{f,TS}$ was longer than that in bulk glycerol and nearly the same as that in glycerol-solvated NaX. In *n*-BuOH $\tau_{f,TS}$ was 2.8 times shorter than that in *t*-BuOH, indicating flexibility of the aliphatic chain. In ACN, $\tau_{f,TS}$ was 3 times shorter than that in MeOH, indicating greater rigidity in MeOH. Both MeOH and ACN coordinate to zeolite cations, but only MeOH can hydrogen bond to surface oxygen atoms located on the walls of the supercage. Therefore, hydrogen bonding creates a more rigid environment. The result in THF shows that solvent size also has an influence on mobility. On the basis of bulk solvent density, 6 THF molecules can fit into the supercage, compared to 12 for MeOH and 10 for ACN. Like ACN, THF can only coordinate to zeolite cations. However, a greater fraction of THF is associated with the zeolite surface.

TABLE 5: Rate Constants for Quenching of Pyrene Fluorescence in PSZ[a]

	$k_q/10^6\ s^{-1}\ M^{-1}$	
	quencher = O_2	
solvent	NaY	USY
MeOH	2.6[b]	1600
H_2O		2500
C_6H_{12}	690	1400
	quencher = nitromethane	
solvent	NaX	NaY
ACN	3.8	3.7
MeOH	1.2	13
H_2O	1.0	4.2
	solvent = methanol	
quencher	NaY	USY
NM	13	230
NP	0.72	38
2M2NP	0.18	16

[a] Values were calculated on the basis of quencher concentrations in the bulk solution bathing the zeolite. [b] Value estimated from the rate of quenching of trapped electrons reported previously.[56]

Quenching Studies. Quenching of pyrene fluorescence by species dissolved in polar solvents bathing the zeolite was explored. The quenchers examined were oxygen and three nitrocompounds varying in size including nitromethane (NM), nitropropane (NP), and 2-methyl-2-nitropropane (2M2NP). Quenching rate constants were evaluated based on Stern−Volmer plots of decay rate versus quencher concentration in the solution bathing the zeolite. For all quenchers examined, the rates of fluorescence quenching in solution are diffusion-controlled with $k_q = 2-2.5 \times 10^{10}\ s^{-1}\ M^{-1}$.[52−54] Rate constants in zeolites were generally lower than those in solution because of differences in concentration or mobility of the quencher, as well as screening effects or dimensionality. Dimensionality can be ignored for comparisons of rate constants in zeolites with similar pore structure, such as the ones used here.

Quenching by O_2. Quenching of pyrene fluorescence by O_2 was not observed in polar-solvated NaX and NaY because bubbling systems with either N_2 or O_2 had little influence on lifetimes. In essence, $[O_2] > 12$ mM cannot be achieved in most liquids at room temperature.[55] However, in NaY-cyclohexane fluorescence quenching was measurable, with $k_q = 6.9 \times 10^8\ s^{-1}\ M^{-1}$ as given in Table 5. In NaX-cyclohexane, rate constants were lower and could not be measured accurately. However, we recently reported the rate constant for quenching of ion cluster trapped electrons in NaX and NaY bathed in cyclohexane as $1.4 \times 10^8\ s^{-1}\ M^{-1}$ and $5.0 \times 10^8\ s^{-1}\ M^{-1}$, respectively.[56] The value in NaY is only slightly lower than the rate of fluorescence quenching. This implies that quenching of trapped electrons is close to diffusion-controlled. Therefore, the rate of singlet quenching in NaX-cyclohexane can be approximated as $1.4 \times 10^8\ s^{-1}\ M^{-1}$.

Unlike the results in ionic zeolites, O_2 quenching in USY was remarkably efficient and only 10−20 times lower than that in solution. The value of $1.6 \times 10^9\ s^{-1}\ M^{-1}$ given for USY-MeOH in Table 5 can be compared to values reported previously

of 1.4×10^4 s^{-1} M^{-1} and 2.6×10^6 s^{-1} M^{-1} for quenching of trapped electrons in NaX and NaY, respectively.[56] Therefore, singlet quenching in USY-MeOH is predicted to be 10^5 and 600 times higher than that in MeOH-solvated NaX and NaY, respectively. However, differences in nonpolar solvents were not that large: only a factor of 2 for USY and NaY; and an order of magnitude at most for USY and NaX. Clearly, the nature of solvent interactions with the zeolite, or chemical properties of the zeolite, make a large contribution to the quenching efficiency. In USY, solvent interactions with the surface are dispersive, regardless of solvent properties, because of the chemical nature of the USY surface. More specific solvent interactions with NaX and NaY result in greater restrictions on solvent mobility, a more rigid environment, and much lowered quenching efficiency, especially in polar solvents. Diffusion through narrow zeolite apertures is likely to be the rate-limiting step. There could very well be differences in mobility through apertures depending on the zeolite and solvent because O_2 does not adsorb to PSZ and therefore cannot displace polar solvents from the apertures. However, solubility factors must also be considered when making comparisons of rate constants. The microviscosity in polar solvated cavities of NaX and NaY is likely to be higher than that in USY. This should lower the solubility. For example, O_2 solubility in bulk glycerol is only 3% of that in bulk MeOH. To this author's knowledge, there are no accurate methods for measuring O_2 solubility in the voids of PSZ. Studies of quenching by nitrocompounds also show more efficient quenching in USY.

Quenching by Nitrocompounds. Nitrocompounds are much more soluble than O_2 in polar solvents. This provides greater flexibility in the measurements of quenching rates by fluorescence. In the current study, samples were submerged in excess solution containing the nitrocompound and allowed to stand for 30 min. Prolonged exposure, up to 4 h, did not affect the results. Prior to measurement, USY samples were bubbled in N_2. In all cases, quenching could be eliminated by thoroughly rinsing samples with neat solvents.

The rate constants in Table 5 show more efficient quenching by nitrocompounds in USY compared to NaX and NaY. Even bulky quenchers such as 2M2NP show higher rates than those measured for NM in NaY. The more efficient quenching in USY suggests that pyrene might be located on the external particle surface of USY. However, this is not case. Pyrene does not adsorb to USY from MeOH. Further, the quenching rates for nitrocompounds in USY are all much smaller than those for O_2. If pyrene was located on the external particle surface, then the quenching rates for NM and O_2 would be similar as they are in solution because both would approach the interface from solution.[54] Therefore, pyrene cannot be located on the external particle surface.

Nitrocompounds have large dipole moments and show high affinity for zeolites in nonpolar solvents.[31] In polar solvents, competition for adsorption sites is expected. To gauge the affinity of NM for NaY in polar solvents, an approach based on the Perrin model of fluorescence quenching was used.[34] Figure 9 illustrates the decay profiles for quenching in NaY-ACN from which dynamic rate constants were assessed. Static quenching can also be seen through lowering of the initial intensity of decay profiles. The static quenching can be explained by occupation of NM in pyrene-occupied supercages during excitation. Dynamic quenching results from cage-to-cage diffusion of NM. According to the Perrin model of static quenching, the initial intensity is related to the number of pyrene-occupied supercages not containing a quencher. The challenge is to predict the occupation number for NM in pyrene-occupied supercages.

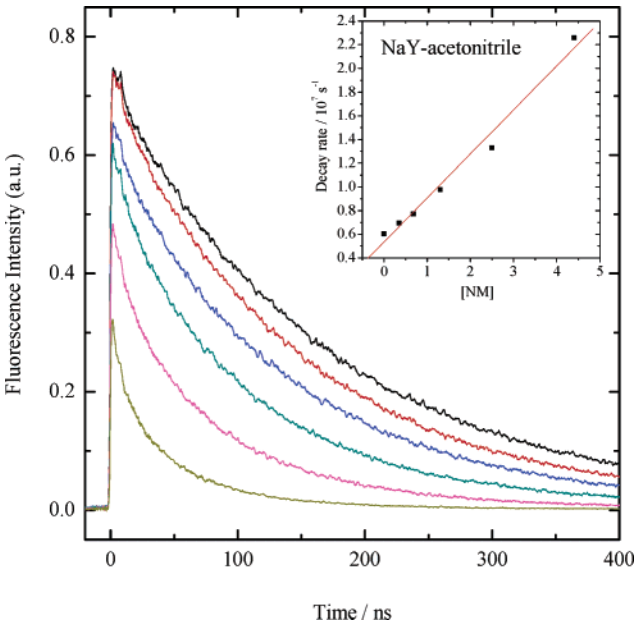

Figure 9. Influence of nitromethane concentration on decay profiles of pyrene fluorescence in NaY-acetonitrile. λ_{ex} = 337 nm; λ_{em} = 372 nm.

If the assumption is made that the concentration of NM in the solution filling the zeolite void volume, excluding the sodalite cages, is the same as that in the solution bathing the zeolite, then the occupation numbers can be predicted by using known values of the zeolite void volume and the supercage concentration. For NaY, these values are given as 0.30 mL g^{-1} (from Breck's book)[40] and 625 μmol g^{-1} (from the unit cell molecular weight), respectively, from which the average occupation number (n_{avg}) of NM can be estimated. For example, at [NM] = 1.0 M in the solution bathing the zeolite, n_{avg} = 0.48. According to Poisson statistics upon which the Perrin model is based, the fraction of supercages containing n quencher, P_n, is given by

$$P_n = \frac{n_{avg}^n e^{-n_{avg}}}{n!}$$

Therefore, at 1.0 M P_0 = 0.62, which states that 62% of the supercages should be unoccupied. Thus, the initial intensity at 1.0 M should be 0.62 times that in the absence of quencher (or I/I_0 = 0.62) if the model and its assumptions are correct.

In Figure 10 values of I/I_0 are plotted versus $[NM]_{soln}$ as measured from decay profiles in NaY, as well as that predicted from the Perrin model based on the assumptions given above. The results in MeOH are in reasonable agreement with the model. However, values of I/I_0 in ACN are slightly higher at a given [NM] than in MeOH. This can be explained by competition for adsorption sites. Because ACN has a higher dipole moment than MeOH, ACN competes more effectively with NM for adsorption sites including cations on the zeolite intraparticle surface. Values measured in water are also included but were limited by the solubility of NM in water.

Values of I/I_0 may be a reasonable predictor of [NM] in NaY. In Figure 11, decay rate is plotted versus I/I_0 and shows that the decay rate is approximately the same at a given I/I_0 regardless of the solvent used. If a given value of I/I_0 is in fact reflective of [NM] in the zeolite void volume, then the similarity of lifetimes at a given I/I_0 implies that the mobility of NM is

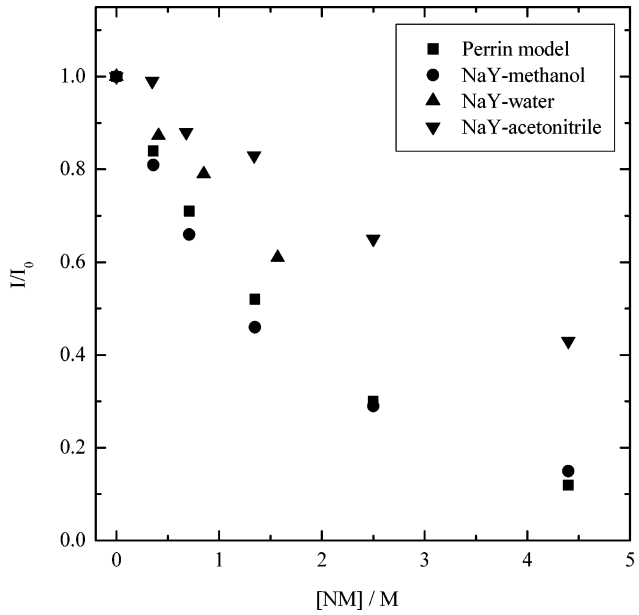

Figure 10. Plots of I/I_0 versus [NM] in polar-solvated NaY. I/I_0 refers to the initial intensity of the pyrene fluorescence decay profile at a given [NM] relative to that in the absence of NM.

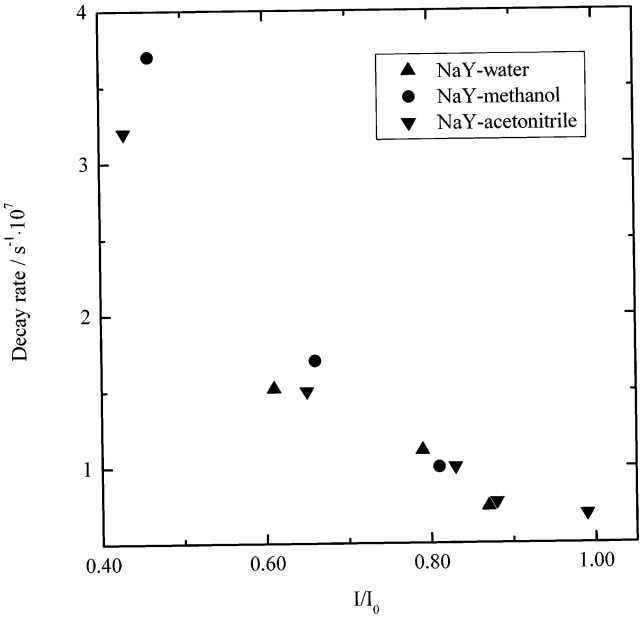

Figure 11. Plots of decay rate of pyrene fluorescence versus I/I_0 for quenching by nitromethane in polar-solvated NaY.

not affected much by the solvent. Therefore, for NaY in Table 5, the differences in quenching rates by NM may only reflect differences in [NM] in the zeolite interior. Plots of decay rate versus I/I_0 were also assessed for NaX. Although not shown in Figure 11, plots for NaX-H_2O and NaX-ACN gave similar values of decay rate to those for NaY. Plots for NaX-MeOH gave lower decay rates, although not by more than a factor of 2. This implies that the mobility of NM in NaX and NaY is similar regardless of the solvent used.

In USY-MeOH, the dynamic rate constant for quenching by NM was 18 times that in NaY-MeOH. The more rapid rate in USY contributed to a significant drop in initial intensity at high NM concentrations needed to achieve static quenching. For this reason, initial intensities at high [NM] could only be obtained by extrapolation. Because this is not a very accurate approach, a study of static quenching in USY was not pursued.

The quenching rates for NM can be compared to those for O_2. The rate constant for singlet quenching by O_2 in NaY-MeOH can be taken as 2.6×10^6 s^{-1} M^{-1}, which is 5 times smaller than the rate for NM. In NaX-MeOH, the O_2 rate was 90 times smaller than the rate for NM. These results point out that adsorption of the quencher makes a significant contribution to the quenching efficiency. Although adsorption definitely affects solubility, it could also affect diffusion because an adsorbing quencher can displace polar solvents from the apertures. The effects of adsorption are more significant in ionic zeolites.

Summary

Fluorescence methodologies have been employed to examine the medium of zeolites interfaced with bathing polar solvents, or polar-solvated zeolites (PSZ). Zeolites X, Y, and USY were compared, all of which have a similar pore morphology. Stark differences in results were found depending on the chemical properties of the zeolite. From measurements of pyrene fluorescence, micropolarity in the supercage of either NaX or NaY bathed in anhydrous polar solvents was found in most cases to be higher than that in the bulk solvent bathing the zeolite. Overall, micropolarity in these systems resembled that in bulk DMF. These results indicate that zeolite exchangeable cations are difficult to avoid in the confines of the supercage, despite the presence of desorbing polar solvents. In USY, micropolarity was generally equivalent to or higher than that in bulk hexanol, and in some cases approached that in bulk hexane. Overall, micropolarity in USY was generally much lower compared to that in the bulk solvent bathing the zeolite, even in very polar solvents such as DMF. These results are in accord with the hydrophobic nature of USY. In essence, micropolarity in PSZ can be described as the combination (or possibly the average) of effects due to bulk solvents and effects due to the zeolite. Such results are expected for probes positioned directly at a liquid−solid interface.

Rates of pyrene fluorescence quenching by O_2 were also found to reflect the chemical nature of the zeolite surface. In USY-MeOH, the rate of O_2 quenching was only 12 times lower than that in bulk MeOH; in NaX-MeOH and NaY-MeOH, this rate was 600 and 10^5 times lower, respectively. These differences can be attributed to the strength of solvent interactions with the zeolite surface. Weak, dispersive interactions of polar solvents with USY give rise to a more fluid medium and greater accessibility of O_2 to entrapped arenes. Stronger ion−dipole and hydrogen bonding interactions of polar solvents with NaX and NaY create a more rigid environment and lowered access of O_2 to the zeolite interior compared to USY.

This study has provided a unique assessment of solvent effects in nanosized pore spaces made possible by retainment of fluorescent arene probes in PSZ. In essence, a liquid−solid interface devoid of overlying bulk solvent has been probed. A clear and important distinction has been made between weakly and strongly interacting solid surfaces. Such information is important in the characterization of liquid−solid interfaces, for describing molecular behavior in confining media, and in the use of zeolites and other microporous solids as reaction media. Currently, we are exploring the medium of PSZ in more detail through studies of photoinduced, bimolecular quenching and electron-transfer involving retained or entrapped arenes. A major goal of the research is to establish how properties of the zeolite and solvent combine to influence the organization and reactivity of neutral donor−acceptor photosystems in zeolite cavities.

Acknowledgment. UM Office of Research and Sponsored Programs.

Supporting Information Available: Additional values of pyrene III/I and fluorescence lifetimes in solvated zeolites and in bulk solvents. This material is available free of charge via the Internet at http://pubs.acs.org.

References and Notes

(1) Thomas, J. K. *Chem. Rev.* **2005**, *105*, 1683.
(2) Ramamurthy, V.; Shailaja, J.; Kaanumalle Lakshmi, S.; Sunoj, R. B.; Chandrasekhar, J. *Chem. Commun.* **2003**, 1987.
(3) Sivaguru, J.; Natarajan, A.; Kaanumalle Lakshmi, S.; Shailaja, J.; Uppili, S.; Joy, A.; Ramamurthy, V. *Acc. Chem. Res.* **2003**, *36*, 509.
(4) Ramamurthy, V.; Turro, N. J. *J. Inclusion Phenom.* **1995**, *21*, 239.
(5) Ramamurthy, V.; Eaton, D. F.; Caspar, J. V. *Acc. Chem. Res.* **1992**, *25*, 299.
(6) Turro, N. J. *Acc. Chem. Res.* **2000**, *33*, 637.
(7) Scaiano, J. C.; Garcia, H. *Acc. Chem. Res.* **1999**, *32*, 783.
(8) Vaidyalingam, A. S.; Coutant, M. A.; Dutta, P. K. Electron-transfer processes in zeolites and related microheterogeneous media. In *Electron Transfer in Chemistry*; Balzani, V., Ed.; Wiley-VCH Verlag GmbH: Weinheim, Germany, 2001; Vol. 4, p 412.
(9) Vasenkov, S.; Frei, H. *Mol. Supramol. Photochem.* **2000**, *5*, 295.
(10) Calzaferri, G.; Maas, H.; Pauchard, M.; Pfenniger, M.; Megelski, S.; Devaux, A. *Adv. Photochem.* **2002**, *27*, 1.
(11) Suib, S. L. *Photochem. Photophys.* **1991**, *3*, 1.
(12) Clennan, E. L. *Mol. Supramol. Photochem.* **2003**, *9*, 275.
(13) Yoon, K. B. *Chem. Rev.* **1993**, *93*, 321.
(14) Yoon, K. B. *Mol. Supramol. Photochem.* **2000**, *5*, 143.
(15) Hashimoto, S. *Mol. Supramol. Photochem.* **2000**, *5*, 253.
(16) Uppili, S.; Thomas, K. J.; Crompton, E. M.; Ramamurthy, V. *Langmuir* **2000**, *16*, 265.
(17) Iu, K. K.; Thomas, J. K. *Langmuir* **1990**, *6*, 471.
(18) Liu, X.; Iu, K. K.; Thomas, J. K. *J. Phys. Chem.* **1989**, *93*, 4120.
(19) Liu, X.; Thomas, J. K. *Langmuir* **1993**, *9*, 727.
(20) Liu, X.; Thomas, J. K. *Chem. Mater.* **1994**, *6*, 2303.
(21) Ellison, E. H.; Thomas, J. K. *J. Phys. Chem. B* **2001**, *105*, 2757.
(22) Ramamurthy, V.; Caspar, J. V.; Corbin, D. R.; Eaton, D. F.; Kauffman, J. S.; Dybowski, C. *J. Photochem. Photobiol., A* **1990**, *51*, 259.
(23) Hashimoto, S.; Ikuta, S.; Asahi, T.; Masuhara, H. *Langmuir* **1998**, *14*, 4284.
(24) Hashimoto, S. *Chem. Phys. Lett.* **1996**, *252*, 236.
(25) Cozens, F. L.; Regimbald, M.; Garcia, H.; Scaiano, J. C. *J. Phys. Chem.* **1996**, *100*, 18165.
(26) Suib, S. L.; Kostapapas, A. *J. Am. Chem. Soc.* **1984**, *106*, 7705.
(27) Thomas, K. J.; Sunoj, R. B.; Chandrasekhar, J.; Ramamurthy, V. *Langmuir* **2000**, *16*, 4912.
(28) Hashimoto, S.; Hagiwara, N.; Asahi, T.; Masuhara, H. *Langmuir* **1999**, *15*, 3123.
(29) Hashimoto, S. *Tetrahedron* **2000**, *56*, 6957.
(30) Ellison, E. H.; Thomas, J. K. *Microporous. Mesoporous. Mater.* **2001**, *49*, 15.
(31) Ellison, E. H.; Thomas, J. K. *Langmuir* **2001**, *17*, 2446.
(32) Ellison, E. H. *J. Phys. Chem. B* **2004**, *108*, 4607.
(33) Zhang, G.; Thomas, J. K. *J. Phys. Chem. B* **2003**, *107*, 7254.
(34) Thomas, J. K. *The Chemistry of Excitation at Interfaces*; American Chemical Society: Washington, D.C., 1984.
(35) Kalyanasundaram, K. *Photochemistry in Microheterogeneous Systems*; Academic Press: New York, 1987.
(36) Kalyanasundaram, K. Photophysical probes for microenvironments. In *Photochemistry in Organized and Constrained Media*; Ramamurthy, V., Ed.; VCH: New York, 1991.
(37) Kalyanasundaram, K.; Thomas, J. K. *J. Am. Chem. Soc.* **1977**, *99*, 2039.
(38) Birks, J. B. *Photophysics of Aromatic Molecules (Wiley Monographs in Chemical Physics)*; Wiley-Interscience: New York, 1970.
(39) Ellison, E. H.; Levidiotis, R. *Microporous Mesoporous Mater.* **2005**, *87*, 192.
(40) Breck, D. W. *Zeolite Molecular Sieves: Structure, Chemistry, and Use*; Wiley-Interscience: New York, 1974.
(41) Halasz, I.; Kim, S.; Marcus, B. *J. Phys. Chem. B* **2001**, *105*, 10788.
(42) Albery, W. J.; Bartlett, P. N.; Wilde, C. P.; Darwent, J. R. *J. Am. Chem. Soc.* **1985**, *107*, 1854.
(43) Krasnansky, R.; Koike, K.; Thomas, J. K. *J. Phys. Chem.* **1990**, *94*, 4521.
(44) Thomas, J. K. *Chem. Rev.* **1993**, *93*, 301.
(45) Chandrasekaran, K.; Thomas, J. K. *J. Colloid Interface Sci.* **1984**, *100*, 116.
(46) Ruetten, S. A.; Thomas, J. K. *J. Phys. Chem. B* **1998**, *102*, 598.
(47) Pankasem, S.; Thomas, J. K. *J. Phys. Chem.* **1991**, *95*, 7385.
(48) Kalyanasundaram, K.; Thomas, J. K. *J. Phys. Chem.* **1977**, *81*, 2176.
(49) Gessner, F.; Olea, A.; Lobaugh, J. H.; Johnston, L. J.; Scaiano, J. C. *J. Org. Chem.* **1989**, *54*, 259.
(50) Kim, S. K.; Courtney, S. H.; Fleming, G. R. *Chem. Phys. Lett.* **1989**, *159*, 543.
(51) Sumitani, M.; Yoshihara, K. *B. Chem. Soc. Jpn.* **1982**, *55*, 85.
(52) Cheng, S.; Thomas, J. K. *Radiat. Res.* **1974**, *60*, 268.
(53) Krasnansky, R.; Thomas, J. K. *J. Photochem. Photobiol. A* **1991**, *57*, 81.
(54) Kavanagh, R. J.; Thomas, J. K. *Langmuir* **1998**, *14*, 352.
(55) Murov, S. L.; Carmichael, I.; Hug, G. L. *Handbook of Photochemistry*; Marcel Dekker: New York, 1993.
(56) Ellison, E. H. *J. Phys. Chem. B* **2005**, *109*, 20424.